ACS Energy LETTERS

http://pubs.acs.org/journal/aelccp

Additive Engineering with Triple Cations and Bifunctional Sulfamic Acid for Tin Perovskite Solar Cells Attaining a PCE Value of 12.5% without Hysteresis

Chun-Hsiao Kuan, Juin-Min Chih, Yu-Cheng Chen, Bo-Hong Liu, Chia-Hsin Wang, Cheng-Hung Hou, Jing-Jong Shyue, and Eric Wei-Guang Diau*

Cite This: *ACS Energy Lett.* 2022, 7, 4436−4442

ABSTRACT: Imidazolium (IM) and cesium (Cs) were treated as A-site cationic additives for a triiodide tin perovskite solar cell ($FASnI_3$; FA, formamidinium) with sulfamic acid (SA) as a bifunctional additive in varied proportions. IM has a tight aromatic structure that is feasible to passivate the crystal defects and help in perovskite crystallization. Cs can stabilize the crystal structure and decrease trap state densities. TOF-SIMS measurements show the passivation effect of both IM and SA occurring on the surface of the film. The bifunctional SA additive can occupy the iodine vacancies in tin perovskites to passivate the uncoordinated Sn atoms and to passivate the surface defects effectively. Furthermore, SA has the effect of reducing Sn^{4+} back to Sn^{2+} via its ammonia/acid form converted from its zwitterionic form upon irradiation, as observed from *in situ* XPS measurements. The hybrid device was optimized to attain a PCE value of 12.5% for the perovskite structure $Cs_{0.02}IM_{0.1}FA_{0.88}SnI_3$+1% SA with superior, long-lasting stability.

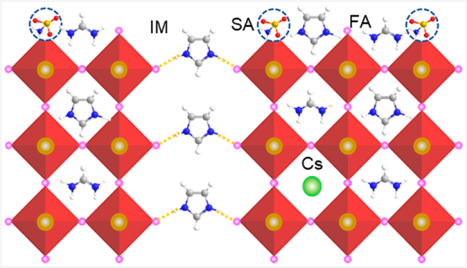

Tin perovskite solar cells (TPSCs) have become some of the most promising candidates for lead-free perovskite solar cells as a next-generation photovoltaic technology.[1−4] However, the intrinsic problems of TPSCs, such as Sn^{2+}/Sn^{4+} oxidation, rapid crystallization, poor stability, and so on, need to be solved to promote the device performance for TPSCs.[5−8] Many approached have been reported to tackle these problems;[9−11] among them, additive engineering is a promising approach to passivate the surface defects, reduce Sn^{4+} back to Sn^{2+}, modulate crystallization, form a surface-protected low-dimensional perovskite, and so forth.[12−16] Tin fluoride (SnF_2) and ethylene diammonium diiodide ($EDAI_2$) are two of the most common additives to prevent Sn^{2+}/Sn^{4+} oxidation as well as to regulate the crystallization for TPSC.[13,17] In addition to these two additives, others such as cationic, anionic, and multifunctional additives have been widely considered for TPSCs.[1,2,18−20] We have previously reported organic cations such as guanidinium (GA),[21] 2-hydroxyethylammonium (HEA),[22] and aziridinium (AZ)[23] as A-site cations to cocrystallize with formamidinium (FA) to form cocationic tin perovskites for enhanced performance and stability for TPSCs. In the present study, a new organic cation, imidazolium (IM), was implemented to mix with FA to form a cocationic tin perovskite. IM is a tight five-membered-ring aromatic molecule with two nitrogen atoms; one can form an H-bond with the SnI_6^{4-} metal halide framework, and the other can serve as a Lewis base to passivate the Sn atoms that were not fully coordinated.[24,25] IM (258 pm) is slightly larger than FA (253 pm) but has a a rigid molecular structure to modulate the perovskite crystal structure with a tolerance factor of close to 1.[26] On the other hand, we also considered incorporating an inorganic cation, cesium (Cs), for its great stability as an A-site cation together with FA and IM to form a Cs/IM/FA triple-cationic tin perovskite system with good performance and stability, as has been reported for its lead analogue.[27−29]

In addition, functional additives such as deoxidizers, surface passivation agents, and crystallization regulators play important roles in decreasing tin(II) oxidation, passivating surface defects, and protecting the perovskite from penetration of

Received: September 21, 2022
Accepted: November 9, 2022

https://doi.org/10.1021/acsenergylett.2c02148
ACS Energy Lett. 2022, 7, 4436−4442

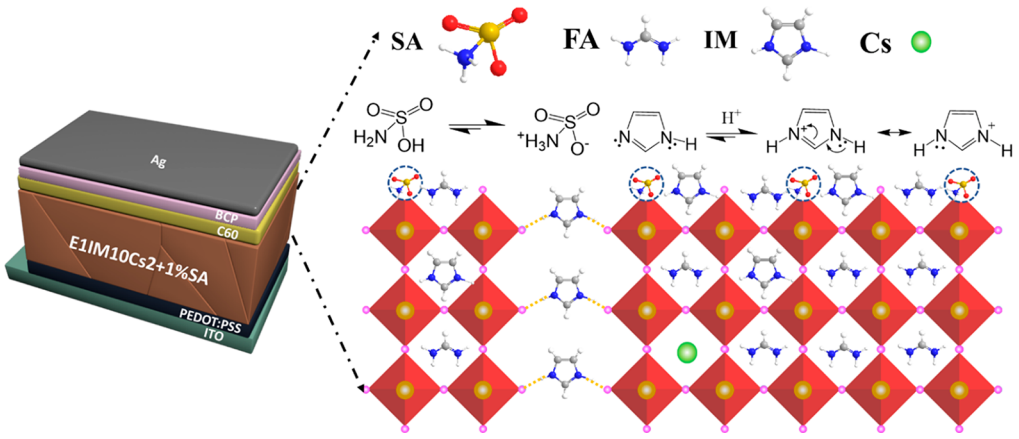

Figure 1. Device structure and functionality demonstration of a tin perovskite solar cell with Cs/IM/FA triple cations and sulfamic acid (SA) as a bifunctional additive.

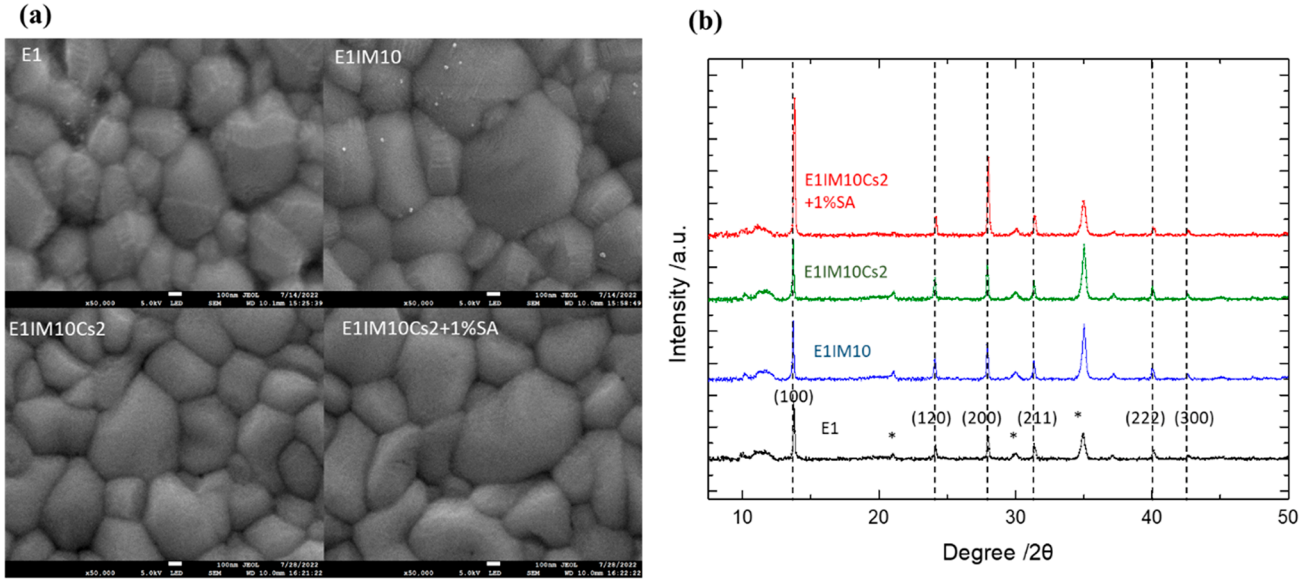

Figure 2. (a) SEM images and (b) XRD patterns of E1, E1IM10, E1IM10Cs2, and E1IM10Cs2 + 1%SA films. The asterisks shown in (b) represent the XRD patterns from the ITO substrate.

moisture.[1,2] Sulfamic acid (SA) has been used to accelerate the conversion of PbI_2 to a lead perovskite, grow large crystals on the substrate, and passivate the crystal defects to prevent its performance degradation.[30] Moreover, SA has been used to align the energy levels of lead perovskites for enhanced charge extraction and device performance.[30] In addition, as a zwitterionic species, SA has the ability to passivate both positive and negative charge defects due to undercoordinated lead and halides and to accelerate electron transfer from the perovskite to the electron-transport layer.[31] Based on the same idea as that for the lead perovskite, we applied SA to our triple-cation tin perovskite system and the device performance has been optimized to give J_{SC} = 22.8 mA cm^{-2}, V_{OC} = 0.74 V, FF = 0.74, and an overall PCE of 12.5%. Figure 1 shows the chemical structures and functionalities of FA, IM, and SA that were incorporated into the TPSC for the best device performance as reported herein.

The TPSC device was fabricated according to a typical inverted device architecture with ITO/PEDOT:PSS/perovskite/C_{60}/BCP/Ag (Figure 1). The perovskite layer was prepared according to a conventional one-step method with four different precursor conditions: (1) E1, 0.85 M (FAI + SnI_2) in DMSO with 10% SnF_2 and 1% $EDAI_2$;[13] (2) E1IM*x*, the same as E1 but with additional IMI in *x*% molar proportion (FAI was adjusted for the molar ratio (FAI + IMI)/SnI_2 = 1), where *x* = 5, 10, 15, and 20; (3) E1IM*x*Cs*y*, the same as E1IM*x* but with additional CsI in *y*% molar proportion (IMI was fixed as determined by (2),and FAI was adjusted for the molar ratio (FAI + IMI + CsI)/SnI_2 = 1), where *y* = 1, 2 and 3; (4) E1IM*x*Cs*y* + *z*% SA, the same as E1IM*x*Cs*y* but with additional SA in *z*% weight proportion with respect to DMSO, where *z* = 0.7, 1, and 2. We first made the E1 device from procedure (1) as our reference cell and then systematically optimized *x*, *y* ,and *z* values one by one from procedures (2)−(4) to reach its best performance. The detailed optimization procedure and the corresponding results are given in Figures S1−S40 and Tables S1−S20 in the Supporting Information. Briefly, the consecutive optimization steps determined the *x*, *y*, and *z* values to be 10, 2 and 1, respectively. Therefore, we discuss herein four different compositions of tin perovskites, namely, E1, E1M10,

https://doi.org/10.1021/acsenergylett.2c02148
ACS Energy Lett. 2022, 7, 4436−4442

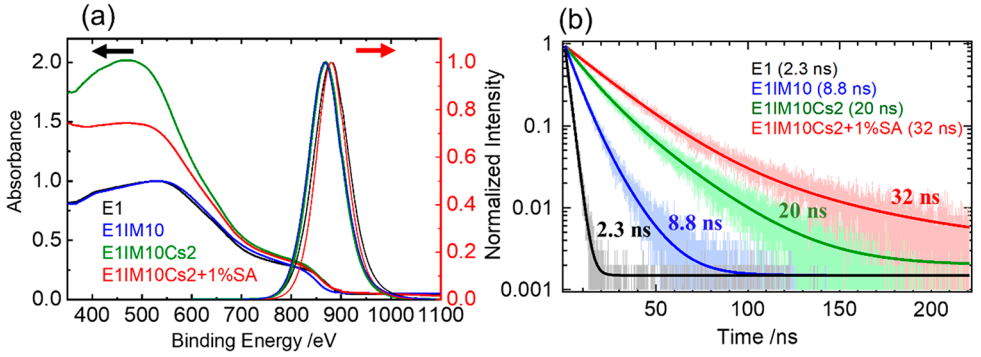

Figure 3. (a) UV−vis/PL spectra and (b) PL transient profiles measured by TCSPC at an excitation wavelength of 635 nm and probed at PL maximum intensity for the four tin perovskite films as indicated.

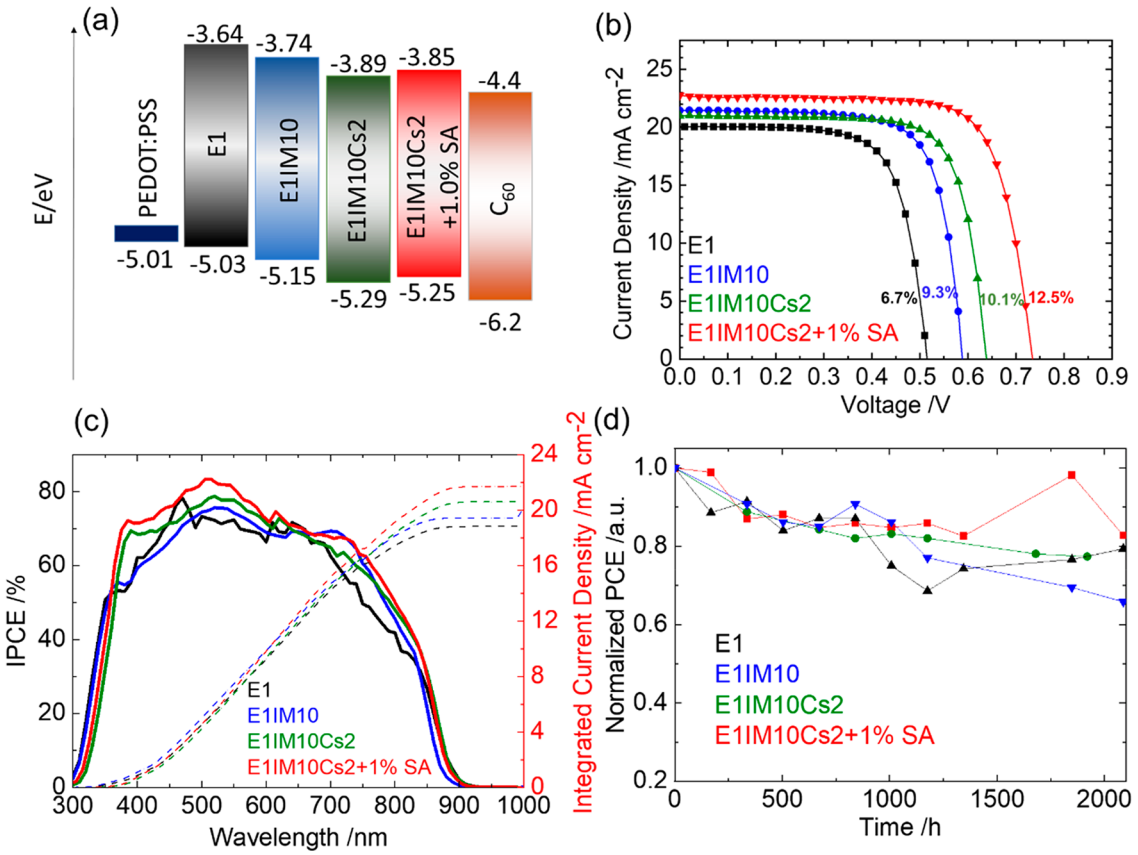

Figure 4. (a) Energy-level diagram, (b) *J*−*V* characteristic curves, (c) IPCE spectra, and (d) long-lasting stability of the devices made of E1, IM10, IM10Cs2 and IM10Cs2 + 1% SA films.

E1M10Cs2, and E1M10Cs2 + 1% SA, for their thin-film characteristics and device performances in what follows.

Figure 2a,b shows SEM images and XRD patterns for these four films, respectively. The SEM images show good morphologies for all films, but with a larger grain size for the E1IM10 and E1M10Cs2 + 1% SA films than for the others. The XRD patterns indicate a slight shift toward smaller diffraction angles for the E1IM*x* films compared to those of the E1 film (Figure S1), as shown by the TOPAS results in Table S1. In contrast, small angular changes toward larger diffraction angles were found for the E1M10Cs*y* films (Figure S10), indicating that the tin perovskite doped with Cs may have a smaller crystal unit size (Table S9). The addition of SA shows a slight change in diffraction angles (Figure S20), and larger crystal sizes were found based on a TOPAS analysis (Table S15). Overall, the crystal size of the E1M10Cs2 + 1% SA film is similar to that of the E1IM10 film but is larger than that of the E1 film. In addition, the intensities of the XRD peaks increase upon consecutive additions of IM, Cs, and SA, with the E1M10Cs2 + 1% SA film showing the greatest crystallinity among the others.

The UV−vis absorption and PL spectra (Figure 3a) show a blue spectral shift with 10% IM, but red spectral shifts occurred when 2% Cs and 1% SA were used. As shown in the PL spectra, the peak positions are located at 880 nm for E1, 865 nm for E1IM10, 872 nm for E1IM10Cs2, and 880 nm for E1M10Cs2 + 1% SA. Urban energy can be determined to show the structural imperfection and defect density of these tin perovskite films. Accordingly, we plot the logarithmic absorbance vs absorption energy to obtain the slope that

https://doi.org/10.1021/acsenergylett.2c02148
ACS Energy Lett. 2022, 7, 4436−4442

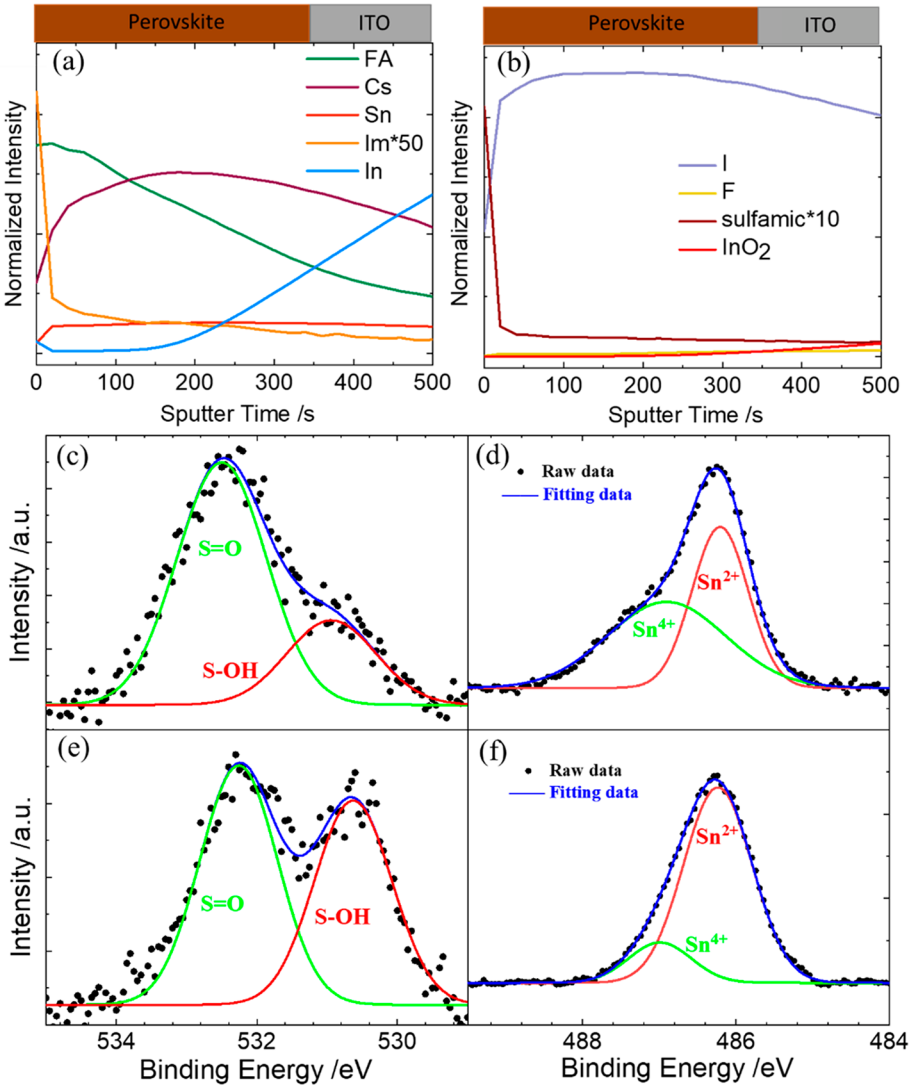

Figure 5. Time-of-flight secondary ion mass spectrometry (TOF-SIMS) depth profiles showing (a) positive and (b) negative ionic signals as a function of sputtering time in the E1IM10Cs2 + 1%SA film. (c, d) *In situ* XPS spectra of O 1s and Sn 3d in the dark, respectively, and (e, f) the corresponding XPS signals under light irradiation for 5 min.

represents the inverse of Urbach energy. As shown in Figure S41, the obtained Urbach energies exhibit the order E1 (62.5 meV) > E1IM10 (61.2 meV) > E1IM10Cs2 (60.6 meV) > E1IM10Cs2 + 1% SA (59.1 meV), indicating the reduced defect concentration with the addition of IM/Cs cations and the sulfamic acid additive. Furthermore, the PL transient profiles shown in Figure 3b exhibit a systematic enhancement in the average decay time coefficients with the trend showing E1M10Cs2 + 1% SA (32 ns) > E1M10Cs2 (20 ns) > E1M10 (8.8 ns) > E1 (2.0 ns). The enhanced PL lifetime for the E1M10Cs2 + 1% SA film indicates that surface and bulk defects were significantly reduced upon incorporation of IM and Cs cations together with the effective SA passivation. Even though the PL lifetime of the SA-treated film has been significantly enhanced, it is still much smaller than those of the lead-based or tin−lead hybrid PSCs.[32−34] This can be rationalized by the small thicknesses of tin perovskites as well as oxidation and tin vacancies inducing defect states[1,2] that are responsible for the much more rapid PL decays for the TPSCs than for the lead or tin−lead PSCs.

Based on the band gap energies determined from the UV−vis spectra and work functions and binding energies determined from the UPS spectra (see the Supporting Information for details), the energy levels for the valence band maximum (VBM) and conduction band minimum (CBM) can be estimated for each tin perovskite species; the corresponding results are shown in Figure 4a. Basically, the incorporation of IM and Cs decreases the VBM and CBM but adding SA slightly increases the energy levels. In all cases, the VBM levels are feasible for hole transfer to the HOMO level of PEDOT:PSS and the CBM levels are feasible for electron transfer to the LUMO level of C_{60}. These perovskite films were fabricated into TPSC devices according to the device structure shown in Figure 1. Figure 4a,b shows the characteristic current density−voltage (J−V) curves and IPCE spectra for all of the devices, for which a systematic trend with E1M10Cs2 + 1% SA (12.5%) > E1M10Cs2 (10.1%) > E1M10 (9.3%) > E1 (7.4%) was observed. Note that the device performance increases mainly due to the enhancement of V_{OC}, which was 0.52 V in E1 but increases to 0.59, 0.64, and 0.74 V in E1M10, E1M10Cs2 and E1M10Cs2 + 1% SA, respectively. The effect

https://doi.org/10.1021/acsenergylett.2c02148
ACS Energy Lett. 2022, 7, 4436−4442

of the V_{OC} enhancement can be understood by the retarded charge recombination, for which the Nyquist plots obtained from the electrochemical impedance spectral (EIS) measurements shown in Figure S42 can explain such an effect. Furthermore, the SA devices show negligible hysteresis, as shown in the forward and reverse $J-V$ curves in Figure S43. Figure 4d shows the long-lasting stability of the devices in the dark for over 2000 h on storage in a glovebox. The device performance slightly degraded upon increasing the storage period, with the SA-treated device showing the best performance at longer storage periods. The stability under light illumination is also an important issue to be addressed. Herein we performed a PCE tracking experiment at the maximum power point for the E1IM10Cs2 + 1%SA device under 1 sun illumination. As shown in Figure S44, the unencapsulated device was stable for 3 h under ambient conditions with 50% humidity.

From our approach, the organic cation IM and the bifunctional additive SA play important roles in boosting the device performance. For IM, it has a five-membered-ring structure with two N−H bonds feasible for passivating undercoordinated Sn atoms and associated charge-trapping defect states. Furthermore, the N−H bonds of IM can form hydrogen bonds with iodine atoms at the grain boundaries to passivate the surface defects, as reported by Jen and co-workers for lead perovskite solar cells (Figure 1).[25] To confirm this surface passivation effect, we performed a time-of-flight secondary ion mass spectrometry (TOF-SIMS) study for the E1M10Cs2 + 1% SA film. Figure 5a shows the TOF-SIMS depth profiles of the cations, for which the IM cations were mainly occupied on the surface area and the IM signal decreases quickly as the sputtering time increases. In contrast, the Cs cations have a lower population on the surface but this gradually increases inside the perovskite crystal. On the other hand, the TOF-SIMS depth profiles of anions shown in Figure 5b indicate that the iodine anions have a lower population on the surface but the I^- signal increases quickly to reach a plateau region inside the crystal. Meanwhile, the SA anions were occupied on the surface and they decreased quickly with the increase in the iodine anions inside the crystal. This phenomenon indicates that the surface of the crystal involves many iodine vacancies that can be occupied by the SA species, as shown in Figure 1. In other words, IM had the effect of passivating the surface defects by forming H-bonds with iodide, whereas SA had the effect of passivating the surface defects by occupying the iodine vacancies and passivating both negatively and positively charged defects due to its zwitterionic feature. Zhang and Zhu have pointed out that electron-donor Lewis bases containing O, S, and N elements can passivate the uncoordinated Pb atoms and ammonium salts can passivate the surface defects for lead perovskites.[35] In our case, the O donor of SA occupied in the iodine vacancies can passivate the uncoordinated Sn atom and the ammonium group in SA can passivate the surface defects for tin perovskites. Therefore, large amounts of IM and SA on the perovskite surface would effectively reduce the defect density and greatly enhance the PL lifetimes to promote an excellent device performance, as we observed herein.

To find out the effect of surface passivation for the SA additive on the effect of the Sn^{2+}/Sn^{4+} oxidation, we carried out *in situ* XPS studies at beamline TLS 24A1, NSRRC, Taiwan, for the E1M10Cs2 + 1% SA film under dark and illumination conditions. Figure 5c,d shows the O 1s and Sn 3d core-level spectra in dark, respectively; Figure 5e,f shows the corresponding XPS spectra under light illumination for 5 min, respectively. Under the dark condition, the relative intensity of the OH bond on the surface is small, whereas the relative intensity of Sn^{4+} is large. However, under light irradiation for 5 min, the Sn^{2+}/Sn^{4+} ratio was significantly enhanced (Figure 5f) while the ratio of S−OH/S═O was also enhanced (Figure 5e) in comparison with those shown under the dark condition (Figure 5c,d). These results indicate that light-induced conversion of SA back to its acid/base form (sulfamic acid) from the zwitterionic form would effectively reduce Sn^{4+} back to Sn^{2+} and this procedure enhances the device performance to a large extent. Since our TOF-SIMS results indicate that most SA species were located on the surface of the film, light irradiation would effectively induce zwitterionic SA to return to sulfamic acid on the iodine vacancies to easily interact with the central tin ion to reduce the Sn^{4+} back to Sn^{2+} on the surface. The SA additive thus plays a key role to prevent Sn^{2+}/Sn^{4+} oxidation and to effectively passivate the tin perovskite surface. As a result, the effect of hysteresis can be reduced due to the limit of ion migration upon SA passivation in the position of iodine vacancies.

Kim et al. pointed out that IM as an A-site additive in lead perovskite might form the 2D structure IM_2PbI_4 with a large band gap.[26] In our case, we wish to know whether or not 10% IM in a tin perovskite layer would produce a 2D/3D structure. To confirm this, we carried out grazing-incidence wide-angle X-ray scattering (GIWAXS) measurements using the facility of beamline TPS 25A1, NSRRC, Taiwan, for the perovskite films made of E1IM5, E1IM10, E1IM20, E1IM40, E1IM80, and E1IM100. The GIWAXS results are shown in Figure S45. The diffraction patterns observed at the (100), (120), (200), (211), (222), and (300) crystal planes (Figure 2b) were unambiguously observed in the GIWAXS patterns for the E1IM5, E1IM10, E1IM20, and E1IM40 films with the expected orthorhombic phase, but then a phase transition occurred to form a δ phase for the E1IM80 and E1IM100 films.[36,37] We did not observe any two-dimensional phase in the bulk 3D tin perovskite crystal with any of the IM-containing films. As shown in Figure S45b, the E1IM10 film exhibits the best crystallinity on the 3D perovskite phase with varied facets compared with the others. Finally, we tested the perovskite film roughness of the E1M10Cs2 + 1% SA film compared with that of the E1 film. As the AFM images show in Figure S46, both films display an average roughness of ∼20 nm, consistent with the uniform crystal morphologies shown in Figure 2a and other SEM images shown in the Supporting Information.

In conclusion, we systematically optimized the crystalline, morphological, optical, optoelectronic, and photovoltaic features for tin perovskite solar cells ($FASnI_3$) via additive engineering through introducing imidazolium (IM) and cesium (Cs) cations together with bifunctional sulfamic acid (SA) in varied proportions. Starting from $FASnI_3$ with 1% $EDAI_2$ additive, the perovskite film quality and device performance were gradually optimized by adjusting the proportion of IM to 10%, the proportion of Cs to 2%, and the weight percentage of SA with respect to DMSO to 1%, giving a device performance for the perovskite with the structure $Cs_{0.02}IM_{0.1}FA_{0.88}$+1%SA attaining a PCE value of 12.5%. The TOF-SIMS results provide strong evidence for surface passivation via IM cations through hydrogen bonding in the grain boundaries and via SA through occupying the iodine vacancies on the surface to passivate the uncoordinated

https://doi.org/10.1021/acsenergylett.2c02148
ACS Energy Lett. 2022, 7, 4436−4442

Sn atom via the O-donor Lewis base of SA and the surface defects via the ammonium group of SA, which were manifested by the systematic enhancement of the PL lifetimes in this series. An *in situ* XPS study further shows the light-induced back reaction from the zwitterionic form converting to the base/acid form, which would play a key role to reduce Sn(IV) back to Sn(II) species. The present study thus reveals the importance of additive engineering to greatly promote the device performance for tin perovskite solar cells using other cationic, anionic, and/or multifunctional additives.

■ ASSOCIATED CONTENT

Supporting Information

The Supporting Information is available free of charge at https://pubs.acs.org/doi/10.1021/acsenergylett.2c02148.

Description of step-by-step optimization procedure, experimental details, and results of XRD, SEM, UV−vis absorption/PL spectra, PL temporal decays, XPS, UPS, energy level diagrams, *J*−*V* curves, IPCE spectra, box plot of photovoltaic parameters, TOPAS analysis, Urbach energy plots, EIS, forward and reverse *J*−*V* scans, MPP tracking plot, and GIWAXS and AFM images (PDF)

■ AUTHOR INFORMATION

Corresponding Author

Eric Wei-Guang Diau − *Department of Applied Chemistry and Institute of Molecular Science and Center for Emergent Functional Matter Science, National Yang Ming Chiao Tung University, Hsinchu 300093, Taiwan;* orcid.org/0000-0001-6113-5679; Email: diau@nycu.edu.tw

Authors

Chun-Hsiao Kuan − *Department of Applied Chemistry and Institute of Molecular Science, National Yang Ming Chiao Tung University, Hsinchu 300093, Taiwan*

Juin-Min Chih − *Department of Applied Chemistry and Institute of Molecular Science, National Yang Ming Chiao Tung University, Hsinchu 300093, Taiwan*

Yu-Cheng Chen − *Department of Applied Chemistry and Institute of Molecular Science, National Yang Ming Chiao Tung University, Hsinchu 300093, Taiwan*

Bo-Hong Liu − *National Synchrotron Radiation Research Center, Hsinchu 30076, Taiwan;* orcid.org/0000-0001-7347-7633

Chia-Hsin Wang − *National Synchrotron Radiation Research Center, Hsinchu 30076, Taiwan*

Cheng-Hung Hou − *Research Center for Applied Sciences, Academia Sinica, Taipei 11529, Taiwan*

Jing-Jong Shyue − *Research Center for Applied Sciences, Academia Sinica, Taipei 11529, Taiwan; Department of Materials Science and Engineering, National Taiwan University, Taipei 10617, Taiwan;* orcid.org/0000-0002-8508-659X

Complete contact information is available at: https://pubs.acs.org/10.1021/acsenergylett.2c02148

Notes

The authors declare no competing financial interest.

■ ACKNOWLEDGMENTS

We thank Dr. E. Jokar and Mr. H.-S. Chuang for their initial efforts on this work. We thank Prof. C.-S. Lin and Ms. Y.-T. Lee of the Instrumentation Center, National Taiwan University, for FEG-SEM experiments. We also thank Dr. Y.-W. Tsai and Dr. J.-M. Lin (NSRRC) for their kind assistance in GIWAXS data analysis. This work was supported by the National Science and Technology Council (NSTC), Taiwan (grant No. NSTC 111-2634-F-A49-007 and NSTC 111-2123-M-A49-001), and the Center for Emergent Functional Matter Science of National Yang Ming Chiao Tung University (NYCU) from The Featured Areas Research Center Program within the framework of the Higher Education Sprout Project by the Ministry of Education (MOE) in Taiwan.

■ REFERENCES

(1) Diau, E. W.-G.; Jokar, E.; Rameez, M. Strategies to Improve Performance and Stability for Tin-based Perovskite Solar Cells. *ACS Energy Lett.* **2019**, *4* (8), 1930−1937.

(2) Jiang, X.; Zang, Z.; Zhou, Y.; Li, H.; Wei, Q.; Ning, Z. Tin Halide Perovskite Solar Cells: an Emerging Thin-Film Photovoltaic Technology. *Acc. Mater. Res.* **2021**, *2* (4), 210−219.

(3) Jiang, X.; Li, H.; Zhou, Q.; Wei, Q.; Wei, M.; Jiang, L.; Wang, Z.; Peng, Z.; Wang, F.; Zang, Z.; et al. One-step Synthesis of SnI_2·$(DMSO)_x$ Adducts for High-Performance Tin Perovskite Solar Cells. *J. Am. Chem. Soc.* **2021**, *143* (29), 10970−10976.

(4) Dai, Z.; Lv, T.; Barbaud, J.; Tang, W.; Wang, T.; Qiao, L.; Chen, H.; Zheng, R.; Yang, X.; Han, L. Stable Tin Perovskite Solar Cells Developed via Additive Engineering. *Sci. China Mater.* **2021**, *64* (11), 2645−2654.

(5) Yu, B. B.; Chen, Z.; Zhu, Y.; Wang, Y.; Han, B.; Chen, G.; Zhang, X.; Du, Z.; He, Z. Heterogeneous 2D/3D Tin-Halides Perovskite Solar Cells with Certified Conversion Efficiency Breaking 14%. *Adv. Mater.* **2021**, *33* (36), 2102055.

(6) Zhu, Z.; Jiang, X.; Yu, D.; Yu, N.; Ning, Z.; Mi, Q. Smooth and Compact $FASnI_3$ Films for Lead-Free Perovskite Solar Cells with over 14% Efficiency. *ACS Energy Lett.* **2022**, *7*, 2079−2083.

(7) Liu, X.; Wu, T.; Zhang, C.; Zhang, Y.; Segawa, H.; Han, L. Interface Energy-Level Management toward Efficient Tin Perovskite Solar Cells with Hole-Transport-Layer-Free Structure. *Adv. Funct. Mater.* **2021**, *31* (50), 2106560.

(8) Liu, X.; Wu, T.; Luo, X.; Wang, H.; Furue, M.; Bessho, T.; Zhang, Y.; Nakazaki, J.; Segawa, H.; Han, L. Lead-Free Perovskite Solar Cells with Over 10% Efficiency and Size 1 cm^2 Enabled by Solvent−Crystallization Regulation in a Two-Step Deposition Method. *ACS Energy Lett.* **2022**, *7* (1), 425−431.

(9) Kuan, C.-H.; Luo, G.-S.; Narra, S.; Maity, S.; Hiramatsu, H.; Tsai, Y.-W.; Lin, J.-M.; Hou, C.-H.; Shyue, J.-J.; Diau, E. W.-G. How Can a Hydrophobic Polymer PTAA Serve as a Hole-Transport Layer for an Inverted Tin Perovskite Solar Cell? *Chem. Eng. J.* **2022**, *450*, 138037.

(10) Shahbazi, S.; Li, M.-Y.; Fathi, A.; Diau, E. W.-G. Realizing a Cosolvent System for Stable Tin-based Perovskite Solar Cells Using a Two-Step Deposition Approach. *ACS Energy Lett.* **2020**, *5* (8), 2508−2511.

(11) Song, D.; Narra, S.; Li, M.-Y.; Lin, J.-S.; Diau, E. W.-G. Interfacial Engineering with a Hole-Selective Self-Assembled Monolayer for Tin Perovskite Solar Cells via a Two-Step Fabrication. *ACS Energy Lett.* **2021**, *6* (12), 4179−4186.

(12) Jokar, E.; Chuang, H.-S.; Kuan, C.-H.; Wu, H.-P.; Hou, C.-H.; Shyue, J.-J.; Wei-Guang Diau, E. Slow Passivation and Inverted Hysteresis for Hybrid Tin Perovskite Solar Cells Attaining 13.5% via Sequential Deposition. *J. Phys. Chem. Lett.* **2021**, *12* (41), 10106−10111.

(13) Jokar, E.; Chien, C.-H.; Fathi, A.; Rameez, M.; Chang, Y.-H.; Diau, E. W.-G. Slow Surface Passivation and Crystal Relaxation with Additives to Improve Device Performance and Durability for Tin-

based Perovskite Solar Cells. *Energy Environ. Sci.* **2018**, *11* (9), 2353−2362.
(14) Jokar, E.; Cheng, P.-Y.; Lin, C.-Y.; Narra, S.; Shahbazi, S.; Wei-Guang Diau, E. Enhanced Performance and Stability of 3D/2D Tin Perovskite Solar Cells Fabricated with a Sequential Solution Deposition. *ACS Energy Lett.* **2021**, *6* (2), 485−492.
(15) Jiang, X.; Wang, F.; Wei, Q.; Li, H.; Shang, Y.; Zhou, W.; Wang, C.; Cheng, P.; Chen, Q.; Chen, L.; et al. Ultra-High Open-Circuit Voltage of Tin Perovskite Solar Cells via an Electron Transporting Layer Design. *Nat. Commun.* **2020**, *11*, 1245.
(16) Narra, S.; Lin, C.-Y.; Seetharaman, A.; Jokar, E.; Diau, E. W.-G. Femtosecond Exciton and Carrier Relaxation Dynamics of Two-Dimensional (2D) and Quasi-2D Tin Perovskites. *J. Phys. Chem. Lett.* **2021**, *12* (51), 12292−12299.
(17) Gupta, S.; Cahen, D.; Hodes, G. How SnF_2 Impacts the Material Properties of Lead-Free Tin Perovskites. *J. Phys. Chem. C* **2018**, *122* (25), 13926−13936.
(18) Chen, M.; Dong, Q.; Eickemeyer, F. T.; Liu, Y.; Dai, Z.; Carl, A. D.; Bahrami, B.; Chowdhury, A. H.; Grimm, R. L.; Shi, Y.; et al. High-Performance Lead-Free Solar Cells based on Tin-Halide Perovskite Thin Films Functionalized by a Divalent Organic Cation. *ACS Energy Lett.* **2020**, *5* (7), 2223−2230.
(19) Wang, C.; Zhang, Y.; Gu, F.; Zhao, Z.; Li, H.; Jiang, H.; Bian, Z.; Liu, Z. Illumination Durability and High-Efficiency Sn-based Perovskite Solar Cell under Coordinated Control of Phenylhydrazine and Halogen ions. *Matter* **2021**, *4* (2), 709−721.
(20) Su, Y.; Yang, J.; Liu, G.; Sheng, W.; Zhang, J.; Zhong, Y.; Tan, L.; Chen, Y. Acetic Acid-Assisted Synergistic Modulation of Crystallization Kinetics and Inhibition of Sn^{2+} Oxidation in Tin-Based Perovskite Solar Cells. *Adv. Funct. Mater.* **2022**, *32* (12), 2109631.
(21) Jokar, E.; Chien, C. H.; Tsai, C. M.; Fathi, A.; Diau, E. W. G. Robust Tin-based Perovskite Solar Cells with Hybrid Organic Cations to Attain Efficiency Approaching 10%. *Adv. Mater.* **2019**, *31* (2), 1804835.
(22) Tsai, C.-M.; Lin, Y.-P.; Pola, M. K.; Narra, S.; Jokar, E.; Yang, Y.-W.; Diau, E. W.-G. Control of Crystal Structures and Optical Properties with Hybrid Formamidinium and 2-Hydroxyethylammonium Cations for Mesoscopic Carbon-Electrode Tin-based Perovskite Solar Cells. *ACS Energy Lett.* **2018**, *3* (9), 2077−2085.
(23) Jokar, E.; Hou, P. H.; Bhosale, S. S.; Chuang, H. S.; Narra, S.; Wei-Guang Diau, E. Mixing of Azetidinium in Formamidinium Tin Triiodide Perovskite Solar Cells for Enhanced Photovoltaic Performance and High Stability in Air. *ChemSusChem* **2021**, *14* (20), 4415−4421.
(24) Zhang, Y.; Grancini, G.; Fei, Z.; Shirzadi, E.; Liu, X.; Oveisi, E.; Tirani, F. F.; Scopelliti, R.; Feng, Y.; Nazeeruddin, M. K.; et al. Auto-Passivation of Crystal Defects in Hybrid Imidazolium/Methylammonium Lead Iodide Films by Fumigation with Methylamine Affords High Efficiency Perovskite Solar Cells. *Nano Energy* **2019**, *58*, 105−111.
(25) Wang, Q.; Lin, F.; Chueh, C.-C.; Zhao, T.; Eslamian, M.; Jen, A. K.-Y. Enhancing Efficiency of Perovskite Solar Cells by Reducing Defects Through Imidazolium Cation Incorporation. *Mater. Today Energy* **2018**, *7*, 161−168.
(26) Kim, J.; Hwang, T.; Lee, B.; Lee, S.; Park, K.; Park, H. H.; Park, B. An Aromatic Diamine Molecule as the A-Site Solute for Highly Durable and Efficient Perovskite Solar Cells. *Small Methods* **2019**, *3* (1), 1800361.
(27) Prasanna, R.; Gold-Parker, A.; Leijtens, T.; Conings, B.; Babayigit, A.; Boyen, H.-G.; Toney, M. F.; McGehee, M. D. Band Gap Tuning via Lattice Contraction and Octahedral Tilting in Perovskite Materials for Photovoltaics. *J. Am. Chem. Soc.* **2017**, *139* (32), 11117−11124.
(28) Lee, J. W.; Kim, D. H.; Kim, H. S.; Seo, S. W.; Cho, S. M.; Park, N. G. Formamidinium and Cesium Hybridization for Photo- and Moisture-stable Perovskite Solar Cell. *Adv. Energy Mater.* **2015**, *5* (20), 1501310.
(29) Kapil, G.; Bessho, T.; Ng, C. H.; Hamada, K.; Pandey, M.; Kamarudin, M. A.; Hirotani, D.; Kinoshita, T.; Minemoto, T.; Shen, Q.; et al. Strain Relaxation and Light Management in Tin−Lead Perovskite Solar Cells to Achieve High Efficiencies. *ACS Energy Lett.* **2019**, *4* (8), 1991−1998.
(30) Guo, Y.; Sato, W.; Shoyama, K.; Nakamura, E. Sulfamic Acid-Catalyzed Lead Perovskite Formation for Solar Cell Fabrication on Glass or Plastic Substrates. *J. Am. Chem. Soc.* **2016**, *138* (16), 5410−5416.
(31) Cao, K.; Huang, Y.; Ge, M.; Huang, F.; Shi, W.; Wu, Y.; Cheng, Y.; Qian, J.; Liu, L.; Chen, S. Durable Defect Passivation of the Grain Surface in Perovskite Solar Cells with π-Conjugated Sulfamic Acid Additives. *ACS Appl. Mater. Interfaces* **2021**, *13* (22), 26013−26022.
(32) Zhu, H.; Trinh, M. T.; Wang, J.; Fu, Y.; Joshi, P. P.; Miyata, K.; Jin, S.; Zhu, X.-Y. Organic Cations Might Not Be Essential to the Remarkable Properties of Band Edge Carriers in Lead Halide Perovskites. *Adv. Mater.* **2017**, *29*, 1603072.
(33) Hu, S.; Otsuka, K.; Murdey, R.; Nakamura, T.; Truong, M. A.; Yamada, T.; Handa, T.; Matsuda, K.; Nakano, K.; Sato, A.; Marumoto, K.; Tajima, K.; Kanemitsu; Wakamiya, A. Optimized carrier extraction at interfaces for 23.6% efficient tin−lead perovskite solar cells. *Energy Environ. Sci.* **2022**, *15*, 2096−2107.
(34) Kapil, G.; Bessho, T.; Sanehira, Y.; Sahamir, S. R.; Chen, M.; Baranwal, A. K.; Liu, D.; Sono, Y.; Hirotani, D.; Nomura, D.; Nishimura, K.; Kamarudin, M. A.; Shen, Q.; Segawa, H.; Hayase, S. Tin−Lead Perovskite Solar Cells Fabricated on Hole Selective Monolayers. *ACS Energy Lett.* **2022**, *7*, 966−974.
(35) Zhang, F.; Zhu, K. Additive Engineering for Efficient and Stable Perovskite Solar Cells. *Adv. Energy Mater.* **2020**, *10*, 1902579.
(36) Sandhu, S.; Singh, R.; Yoo, K.; Kumar, M.; Lee, J.-J. Effect of Binary Additives in Mixed 2D/3D Sn-based Perovskite Solar Cells. *J. Power Sources* **2021**, *491*, 229574.
(37) Zhang, Y.; Wang, Y.; Yang, X.; Zhao, L.; Su, R.; Wu, J.; Luo, D.; Li, S.; Chen, P.; Yu, M.; et al. Mechanochemistry Advances High-Performance Perovskite Solar Cells. *Adv. Mater.* **2022**, *34* (6), 2107420.

https://doi.org/10.1021/acsenergylett.2c02148
ACS Energy Lett. 2022, 7, 4436−4442